Study of hybrid energy system coupling fuel cell, solar thermal system and photovoltaic cell

Ahmad Haddad, Mohamad Ramadan, Mahmoud Khaled, Haitham Ramadan, Mohamad Becherif

Version of Record: https://www.sciencedirect.com/science/article/pii/S0360319918317993
Manuscript_8efddf006c8fd7cb8c89de3cabb2227a

STUDY OF HYBRID ENERGY SYSTEM COUPLING FUEL CELL, SOLAR THERMAL SYSTEM AND PHOTOVOLTAIC CELL

Ahmad Haddad[1], Mohamad Ramadan[1,2 *], Mahmoud Khaled[1,3], Haitham Ramadan[4,5] and Mohamad Becherif[5]

[1] School of Engineering, International University of Beirut, PO Box 146404 Beirut, Lebanon.

[2] Associate member at FCLAB, CNRS, Univ. Bourgogne Franche-Comte, Belfort cedex, France.

[3] Univ. Paris Diderot, Sorbonne Paris Cité, Interdisciplinary Energy Research Institute (PIERI), Paris, France.

[4] Zagazig University, Faculty of Engineering, Electrical Power and Machines Dept., 44519, Zagazig, Egypt.

[5] FEMTO-ST UMR CNRS 6174, FCLab FR CNRS 3539, UTBM, 90010 Belfort cedex, France.

Corresponding author: mohamad.ramadan@liu.edu.lb

Abstract

The present work examines the combination of solar energy systems with Fuel cell. Indeed, fuel cells are green storage systems without any pollution effects. They are supplied by oxygen and hydrogen to produce electricity. That is why it is inescapable to find a source of hydrogen in order to use fuel cell. Several techniques can be adopted to produce hydrogen depending on the availability and the cost of the sources. One of the most utilized techniques is electrolysers. They allow to obtain hydrogen from water by several technologies among them proton exchange membrane (PEM) which is considered in this work. On the other hand, electrolysers need electrical power to operate. A green-green energy system can be constructed by using a renewable energy source to supply fuel cell trough electrolysers. A comparison between two solar systems (Photovoltaic and Parabolic Trough) coupled to fuel cell is performed. A case study on the Lebanese city of Tripoli is carried out. The study shows the performance of each of both combined systems for different parameters and proposes recommendations depending on the considered configuration.

Keywords: Green-Green, Hybrid Renewable Energy, Fuel Cell, Hydrogen Energy, Photovoltaic, Solar Thermal, Optimum Coupling.

1 INTRODUCTION

In the last decades, the domain of energy has undergone a huge revolution. Indeed, the high cost of fuel, the depletion of fuel reserves and the pollution, have direct influence on the current energy crisis. Traditionally the focus of energy studies, concerns mainly the economic dimension. Nonetheless, the dangerous levels of pollution have shed light on the environmental impact of the crisis. On the other hand, a simple anatomy of any energy supply strategy leads to two fundamental parts: energy source and energy storage. Huge efforts have been concentrated to find green sources of energy. To put it

another way, the main objective of energy studies is to assess renewable and sustainable energy systems such as solar energy systems in its two types photovoltaic and solar thermal systems [1-5]. Other works [6-12] concern energy recovery, energy management and energy storage. Fuel cell [13-16] can be seen as a green energy storage system since it is a pollution free device. It uses hydrogen [17-21] to produce electricity. In this frame, many works have been dedicated to assess techniques enhancing hydrogen production [22-28]. Furthermore, processes involving conversion to hydrogen are also investigated. In [29] the authors examine the effect of several parameters on the yields of H2 and methane conversion. Having said that, Green-Green System (GGS) can be constructed by coupling renewable energy source and fuel cell. Figure 1 provides an illustration about the concept of (GGS).

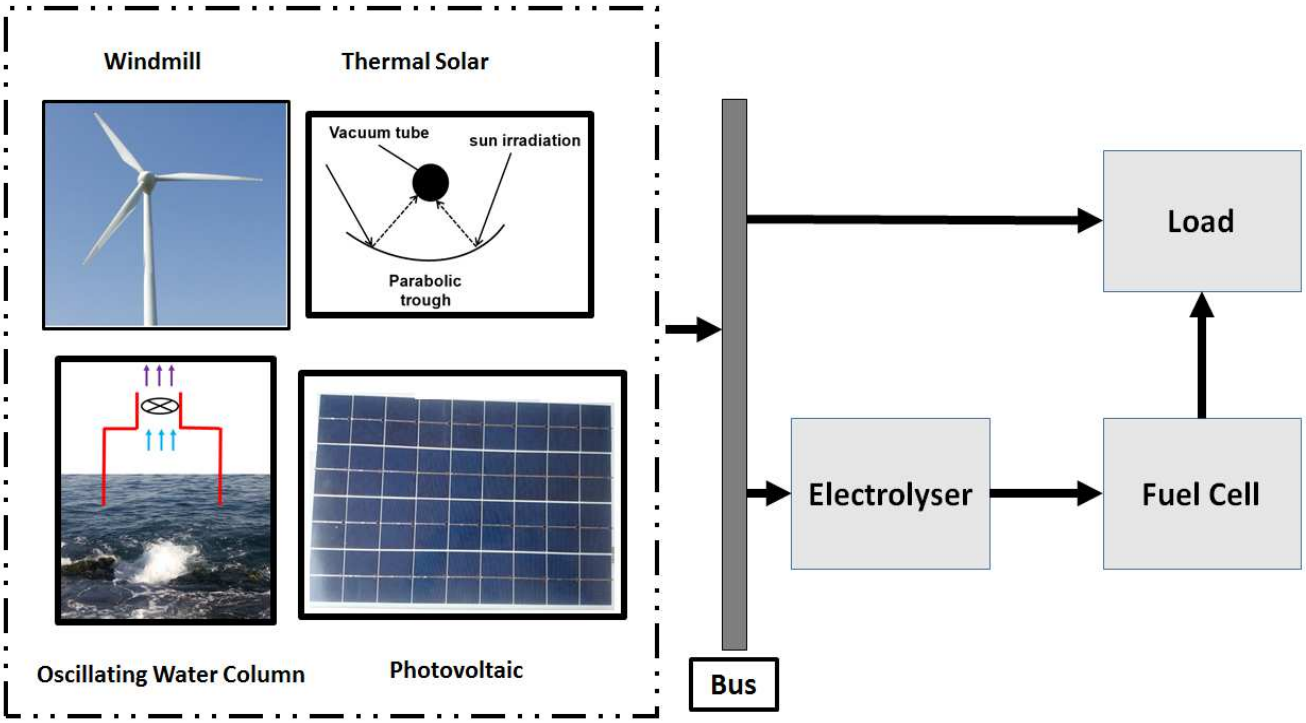

Figure 1: Green-Green energy system

In the light of green-green concept, several studies have been proposed to investigate the coupling of fuel cell with solar energy systems (see figure 2). Indeed, solar energy could be harvested through different systems that generate electricity either directly such as photovoltaic (PV) system or indirectly such as solar thermal (ST) system. With this in mind, selecting the optimal solar system that could be coupled with fuel cell depends on several parameters such as the available area, the cost of investment and the amount of produced power.

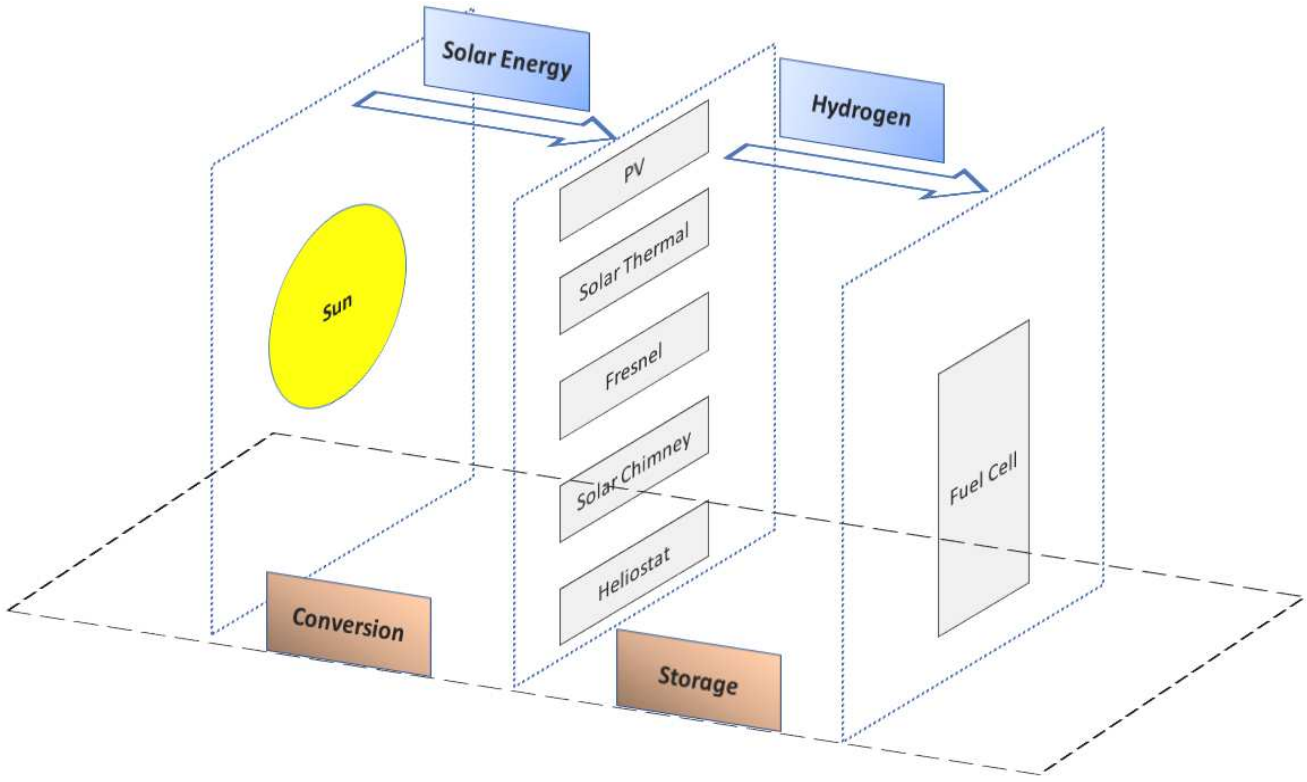

Figure 2. Coupling between solar energy systems and fuel cell

Coupling photovoltaic cell with fuel cell [30-32] is the most investigated solar-fuel cell coupling. In [33] the authors investigate a hybrid system combining photovoltaic, PEM fuel cell, Li-ion battery and ammonia electrolyte cell for vehicle application. That said other studies investigate solar-fuel cell coupling for specific conditions and location as in [34] where the authors assess the use of a solar-fuel cell hybrid system in the Canadian city of Toronto. Ramadan et al [35], propose a system coupling solar thermal system and fuel cell. The solar system is used to power an electrolyser that supplies the fuel cell by hydrogen. The study examines the power supply in terms of the efficiency of the solar system on a daily basis.

By reviewing the existing works in the literature, that suggest (GGS) coupling fuel cell and solar energy, it is remarked that none of the existing works evaluates the performance of the coupling in terms of the adopted solar system. In contrary all the existing papers consider a sol solar system and focus on the coupling procedure. From here is born the motivating spark of this paper which aims to call into question, comparison between two different approaches of coupling solar energy and fuel cell: Photovoltaic-Fuel cell and Solar Thermal-Fuel cell. The aim is to identify the best coupling approach for an imposed criterion. The remaining of the paper is organized as follows: Section two is devoted to present the general procedure of coupling. Modelling of PV, ST, electrolyzer and FC are presented in section three. Results are discussed in section four and concluding remarks are presented in the last section.

2 PROCEDURE OF OPTIMIZATION

Coupling solar energy and FC is performed indirectly through electrolyzer. Indeed, Fuel cell is supplied by hydrogen to provide electricity. That is why it is unescapable to find a source of hydrogen in order to use fuel cell. Several techniques can be adopted to produce hydrogen depending on the availability and the cost of the sources. One of the most utilized techniques are electrolyzers. They allow to obtain hydrogen from water by several technologies among them proton exchange membrane (PEM) which is considered in this work. Having said that, electrolyzers need electrical power to operate. A full green energy system can be constructed by using a renewable energy source to supply electrolyzers. When solar energy is adopted to produce hydrogen. The two main technologies that can be utilized are photovoltaic cell and solar thermal system. The output power delivered by each system varies depending on specific parameters. With this in mind, the optimum solar-fuel cell coupling requires to define a calculation procedure that converges toward the optimal design. Notwithstanding, a decision criterion should be imposed. To this end several criteria could be adopted depending on the objective of the application. In the shade of this paper three criteria are presented. *Total Energy*, *Minimum Threshold* and *Maximum Power Fixed Period*. *Total Energy* is the most generalized criterion since it represents the net provided energy regardless the minimum or maximum power that may be obtained by zooming on a specific period of time. By contrast *Minimum Threshold* does not compare the total energy, it identifies globally the most secured system or in other words the design that provides a power supply greater than a minimum limit. That said, the third criterion or *Maximum Power Fixed Period* is dedicated for application where maximum power is needed for a determined period of time regardless the total energy supplied over the year. The procedure of optimization is illustrated in the flowchart of figure 3.

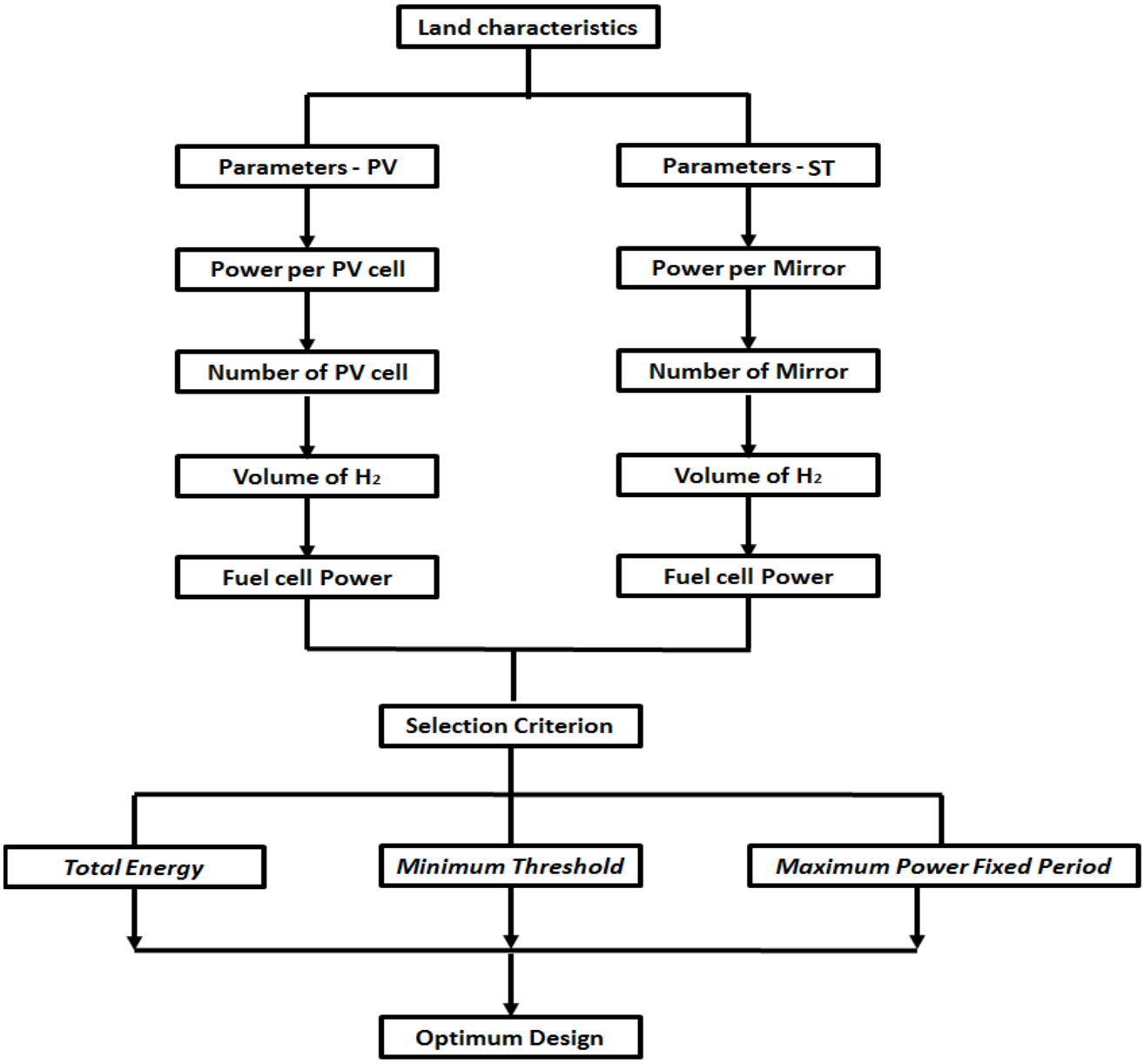

Figure 3. Procedure of optimization

3 PV ARRAY SIZING AND MODELING

The scenario considered in this work, consists on sizing and modeling the PV array system based on a preset land area. This section is divided into two parts: The first part deals with the PV array sizing according to the effective land area, the PV module tilt angle at the selected location, and to the system's DC bus voltage. The second part include the mathematical modeling aiming to calculate the PV array output power with respect to the Direct Normal Insulation (*DNI*) of the selected location and the number of PV modules.

3.1 PV array sizing

In this part, a rectangular land of 1000 m^2 area is considered. The location studied is Tripoli (located in the north of Lebanon: Latitude: 34°26'13" North - Longitude: 35°49'26" East). Solar insulation data for the selected location are taken from the Photovoltaic Geographical Information System (PVGIS).

According to these data, the optimal tilt angle for the selected place is $\theta_{optimal} = 30°$. This is close to the mean tilt angle $\theta_{mean} = 34°$ calculated in Table 1. The PV module used in the array design is the Sunmodule SW 250 mono. Its characteristics are given in Table 2.

Table 1. Mean tilt angle of the PV module

Date	**Latitude** ϕ	**Declination angle of the sun** δ	**PV module tilt angle** $\theta = \phi - \delta$
Dec. 21st	34°	−23°	57°
Mar. 20th	34°	0°	34°
Jun. 21st	34°	+23°	11°
Sep. 23rd	34°	0°	34°
			θ_{mean} = 34°

Table 2. PV module characteristics

Description	**Rating**
Rated power	$P_{max} = 250\ W$
Open circuit voltage	$V_{OC} = 37.8\ V$
Max. power point voltage	$V_{MP} = 31.1\ V$
Short circuit current	$I_{SC} = 8.28\ A$
Max. power point current	$I_{MP} = 8.05\ A$
Dimensions	$167.5\ cm \times 95.1\ cm$

To avoid shading in solar array, a minimum spacing distance D between modules is required as shown in Figures 4 and 5. The shadow distance D is found through using simple trigonometry as follows:

$$D = \frac{h \times \cos(\psi - 180°)}{\tan(\alpha)} \qquad (1)$$

where, h is the height of obstruction calculated from the tilted module length x and the PV module tilt angle θ as shown in Figure 4, α is the solar altitude angle and ψ the solar azimuth angle as shown in Figure 5.

$$h = x \times \sin(\theta) \qquad (2)$$

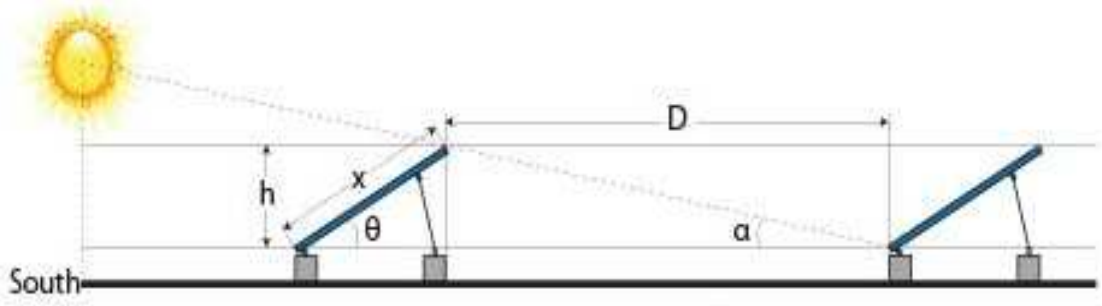

Figure 4. Shadow distance

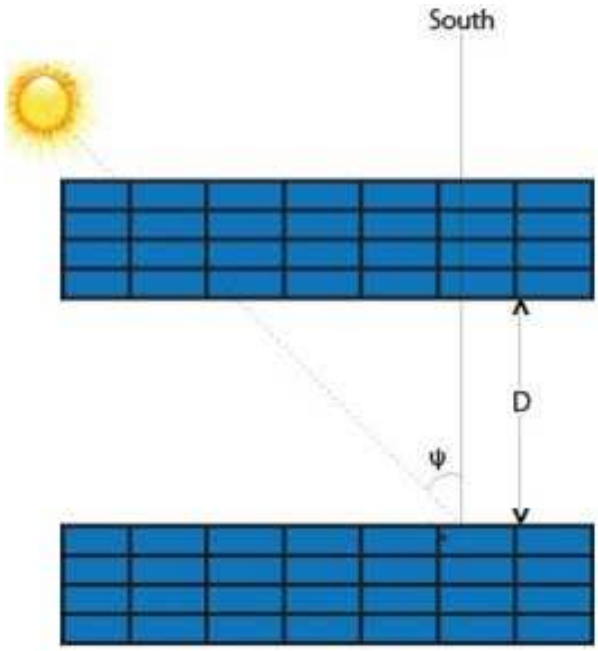

Figure 5. Solar azimuth angle

Given the module length $x = 167.5cm$, the tilt angle $\theta_{optimal} = 30°$, the solar altitude angle considered at the end of the effective sun hours in the worst day of the year (Dec. 21st) $\alpha = 20°$ and the solar azimuth angle under the same conditions $\psi = 229°$, the shadow distance D is:

$$D = \frac{167.5 \sin(30°) \cos(229° - 180°)}{\tan(20°)} = 149cm \qquad (3)$$

Based on the shadow distance D, the PV module dimensions and the optimal tilt angle, the maximum number of PV modules that can fit in $1000\, m^2$ land area is $N_{PV} = 200$ modules. The number of modules in series $N_{PV-Series}$ is the ratio of the array's DC voltage $V_{DC-Array}$ over the module's maximum power point voltage V_{OC} rounded to the next higher integer. To be compatible with the electrolyzer's DC input voltage, we consider $V_{DC-Array} = 150V$. Therefore,

$$N_{PV-Series} = \left.\frac{V_{DC-Array}}{V_{OC}}\right|_{Rounded} = 5\ Modules \quad (4)$$

Hence, the number of modules in parallel $N_{PV-Parallel}$ is:

$$N_{PV-Parallel} = \frac{N_{PV}}{N_{PV-Series}} = 40\ Modules \qquad (5)$$

Figure 6 shows the PV array configuration inside the 1000 m^2 land area.

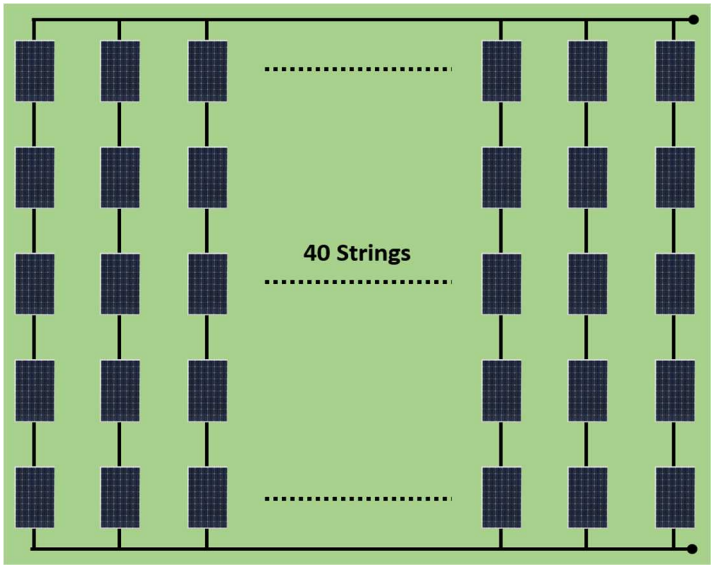

Figure 6. PV array configuration

3.2 PV array mathematical modeling

To elaborate the mathematical modeling of the PV array, we propose to represent the module by the equivalent electrical circuit shown in Figure 7. In fact, the PV module can be seen as a dependent current source controlled by Direct Normal Insulation (*DNI*). This notion is modeled as a photocurrent I_{PH}. Besides, the module is composed of 60 PN junction cells in series which behave as Diode. The movement of current through the emitter and base of the solar cell, the contact resistance between the metal contact and the silicon and the resistance of the top and rear metal contacts cause a drop in the module's voltage. A series resistance R_S is used to represent this drop. In addition, manufacturing defects cause some power loss that is represented with a shunt resistance R_{SH} in parallel.

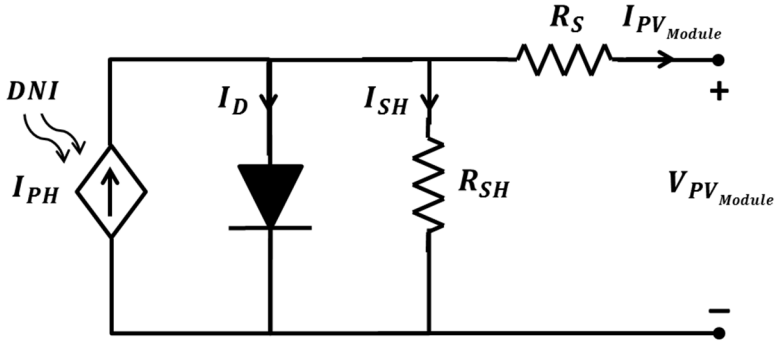

Figure 7. PV module equivalent circuit

The mathematical model of the entire array is given by the block diagram in Figure 8. The main inputs are the *DNI*, the module's temperature T_M, the number of series modules in one string $N_{PV-Series}$, the number of parallel strings in the array $N_{PV-Parallel}$, as well as the module's operating voltage $V_{PV_{Module}}$. The latter is considered as input because it is set by the controller so that to extract maximum power from the module. The outputs are PV array's voltage, current and power.

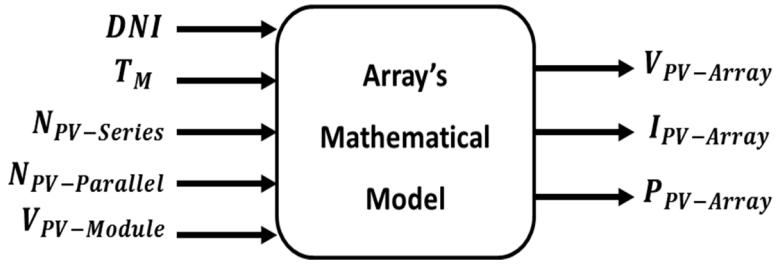

Figure 8. Block diagram of the model

According to the circuit in Figure 7, the module's output current is:

$$I_{PV_{Module}} = I_{PH} - I_D - I_{SH} \quad (6)$$

with I_{PH} : Module's photocurrent given by:

$$I_{PH} = \left[I_{SC} + K_i\left(T_M - T_{ref}\right)\right] \times \frac{DNI}{1000} \quad (7)$$

I_D : Module's diode current given by:

$$I_D = I_S\left[exp^{\left(q \times \frac{V_{PV_{Module}} + R_S I_{PV_{Module}}}{K n T_M}\right)} - 1\right] \quad (8)$$

I_{SH} : Module's current loss caused by its shunt resistance R_{SH}. It is given by:

$$I_{SH} = \frac{V_{OC}}{R_{SH}} \quad (9)$$

where, K_i is temperature coefficient, T_{ref} reference temperature, I_S is module's saturation current, I_{RS} is module's reverse saturation current, q is quantity of electronic charge, E_g energy band gap for the monocrystalline silicon used in the PV module, n is module's ideality factor, K is Boltzmann's constant and R_S is equivalent series resistance of the module.

The total output voltage of the PV array is:

$$V_{PV_{Array}} = N_{PV-Series} \times V_{PV_{Module}} \quad (10)$$

The total output current of the PV array is:

$$I_{PV_{Array}} = N_{PV-Parallel} \times I_{PV_{Module}} \quad (11)$$

The total output power of the PV array is:

$$P_{PV_{Array}} = V_{PV_{Array}} \times I_{PV_{Array}} \quad (12)$$

4 ELECTROLYZER SIZING AND MODELING

To meet the load demand at night and during periods of low insulation, energy storage is essential. Conventional battery bank concept used in small scale projects do not apply in case of large power generation. Indeed, controlling the state of charge of a big battery bank to protect it against overcharge/overdischarge is a challenging problem. Furthermore, batteries' lifetime is limited and harmfully affected with temperature increase. Moreover, they are not environmentally friendly. For all these reasons we propose to use hydrogen production as a storage medium. For this end, we use an electrolyzer of $18kW$ rated power and $150V$ DC voltage. The electrolyzer is sized based on the

maximum DC power produced by the PV array and the Parabolic Trough (PT) system in June with an additional 20% security margin. The hydrogen and oxygen production rates $\dot{m}_{H_2}$ and $\dot{m}_{O_2}$ are:

$$\dot{m}_{H_2} = 2\dot{m}_{O_2} = \frac{n_{cells} \times i_E \times \eta_F}{2\,F} \times 3600 \times \frac{M_{H_2}}{\rho_{H_2}} \quad (13)$$

with, n_{cells} is number of electrolyzer's cells, F Faraday's constant, M_{H_2} molar mass of hydrogen, ρ_{H_2} density of hydrogen and η_F Faraday's efficiency given by:

$$\eta_F = 96.5 \times exp^{\left(\frac{0.09}{i_E} - \frac{75.5}{i_E^2}\right)} \quad (14)$$

where i_E is electrolyzer's current given by:

$$i_E = \frac{P_{PV_{Array}}}{150\,V}\ (PV\ case) \quad (15)$$

$$i_E = \frac{P_{PT} \times \eta_{Rectifier}}{150\,V}\ (PT\ case) \quad (16)$$

where $\eta_{Rectifier}$ is rectifier's efficiency. In case of PT, the AC power is converted to DC using a rectifier.

5 FUEL CELL SIZING AND MODELING

Hydrogen and oxygen produced by the electrolyzer are used to feed the Fuel Cell system for power generation in absence of solar radiations. The fuel cell's output current [36] is function of hydrogen consumption rate as shown in the following equation:

$$i_{FC} = \frac{2\,F \times \dot{m}_{H_2}}{3600} \times \frac{\rho_{H_2}}{M_{H_2}} \quad (17)$$

The output voltage per cell is:

$$V_{cell} = E_{nernst} - V_{act} - V_{ohm} - V_{conc} \quad (18)$$

with E_{nernst} the open circuit voltage, V_{act} the activation voltage loss given by:

$$V_{act} = \frac{R_G\,T_{FC}}{2\,F} \times ln\left(\frac{i_{FC}}{i_0}\right) \quad (19)$$

where, R_G is the gas constant, T_{FC} is the fuel cell temperature, i_0 is the exchange current and V_{ohm} is the ohmic voltage loss given by:

$$V_{ohm} = (R_A + R_M + R_C) \times i_{FC} \quad (20)$$

where, R_A is the Anode electrical resistance, R_C is the cathode electrical resistance, R_M is the membrane electrical resistance and V_{conc} is the concentration voltage loss given by:

$$V_{conc} = \frac{R_G\,T_{FC}}{2\,F} \times ln\left(1 - \frac{i_{FC}}{i_{max}}\right) \quad (21)$$

Where, i_{max} is the limit Current.

The fuel cell's output power is:

$$P_{FC} = V_{FC} \times i_{FC} = N_{cells} \times V_{cell} \times i_{FC} \quad (22)$$

With N_{cells} is the number of cells.

The fuel cell is sized according to its maximum limit current density as well as to the inverter's input DC voltage. Based on experimental works, the maximum limit current density j_{max} of the fuel cell is $0.7A/cm^2$ and the minimum guaranteed fuel cell's output voltage is $0.6V/cell$. According to the maximum DC power produced by the PV array and the PT system in June with an additional 20% security margin, the fuel cell's maximum current is $192A$. Therefore, the cell's area is:

$$A_{cell} = \frac{192\ A}{0.7\ A/cm^2} \approx 275\ cm^2 \qquad (23)$$

The DC input voltage of a conventional $220VAC$ inverter is $48VDC$. Hence, the number of cells is:

$$N_{cells} = \frac{48\ V}{0.6\ V/cell} = 80\ cells \qquad (24)$$

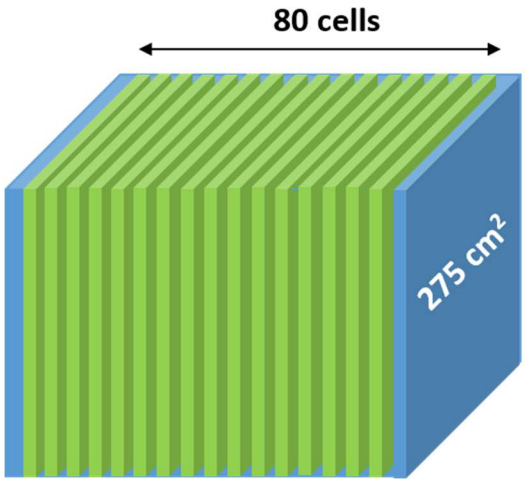

Figure 9. Fuel cell stack sizing

6 PARABOLIC TROUGH SIZING AND MODELING

The received solar energy can be calculated as follows [29]:

$$\dot{Q}_{absorbed} = P_{SUN} . P_{PERFORMANCE} . P_{CONFIGURATON} \qquad (25)$$

where P_{SUN}, $P_{PERFORMANCE}$ and $P_{CONFIGURATION}$ represent respectively parameters of sun irradiance, parameters of performance and parameters of system configuration.

$$P_{SUN} = DNI . \cos\theta . IAM \qquad (26)$$

where the direct normal insulation *DNI* represents the portion of solar radiation that reaches the surface of the earth. It depends generally on time period of the year and location. *IAM* is the incidence angle modifier and θ is the angle of incidence.

$$P_{PERFORMANCE} = Rowshadow . Endloss . \eta_{field} . \eta_{HCE} \qquad (27)$$

where *Rowshadow* accounts for mutual shading. *Endloss* accounts for losses from ends of the receiver tubes or Heat Collection Elements HCE. η_{field} is an efficiency that represents losses due to mirrors' imperfections. η_{HCE} is an efficiency that represents HCEs' imperfections.

$$P_{CONFIGURATION} = SF_a . A \qquad (28)$$

where A is the area of the tube and SF_a is the fraction of the solar field tracking the sun. The angle of incidence is written:

$$\cos\theta = \sqrt{\cos^2\theta_z + \cos^2\delta \sin^2 w} \quad (29)$$

where w represents the hour angle obtained from:

$$\cos\theta_z = \cos\delta\cos\phi\cos w + \sin\delta\sin\phi \quad (30)$$

where $\emptyset$ is the latitude. *IAM* accounts for the additional reflection and absorption losses due to the increase of the angle of incidence:

$$IAM = \frac{K}{\cos\theta} \quad (31)$$

$$K = \cos\theta + 0.000884\theta + 0.00005369\theta^2 \quad (32)$$

The *Rowshadow* reduces the performance of the collector by reducing the amount of radiation incident:

$$Rowshadow = \frac{L_{spacing}}{W}\frac{\cos\theta_z}{\cos\theta} \quad (33)$$

where W represents the collector aperture width and $L_{spacing}$ represents the spacing length between troughs. Endlosses are characterized by the *Endloss* factor can be determined as follows:

$$Endloss = 1 - \frac{f\tan\theta}{L_{SCA}} \quad (34)$$

where f represents the focal length and L_{SCA} represents the length of single collector assembly. The output electrical power obtained from one mirror is written:

$$P_{mirror} = \dot{Q}_{absorbed} \cdot \eta_{thermal} \cdot \eta_{electrical} \quad (35)$$

where $\eta_{thermal}$ is the thermal efficiency of the cycle and $\eta_{electrical}$ represents the electrical efficiency.

7 SIMULATION RESULTS

The PT output power is AC while the one of PV is DC. In order to compare the two systems, an inverter is used to convert the DC power of the PV array to an AC one. The AC output power of the inverter is:

$$P_{Inverter} = P_{PV_{Array}} \times \eta_{Inverter} \quad (36)$$

with $\eta_{Inverter}$: The inverter's efficiency.

Figure 10 presents the yearly PV and PT AC powers variation based on *DNI* data of the studied location for 1000m^2 land area and an array composed of 1 row.

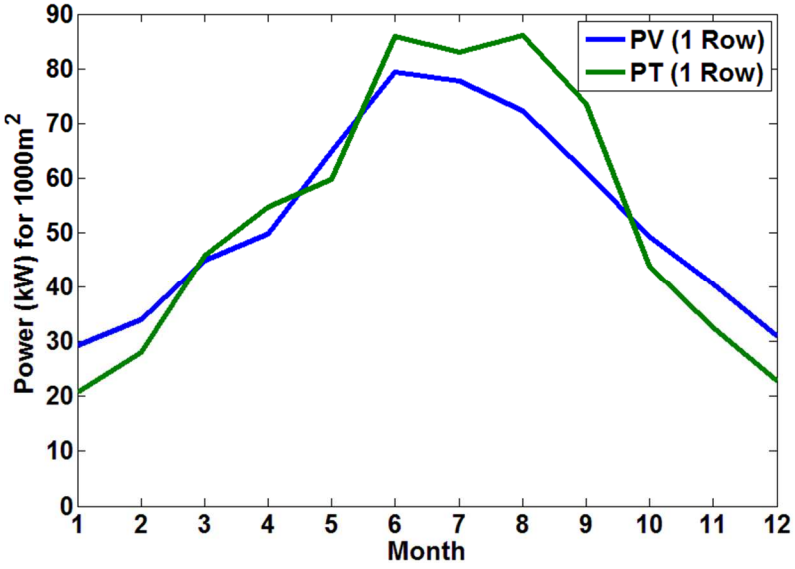

Figure 10. Yearly PV and PT AC powers variation for 1000m^2 with 1 row.

Results in Figure 10 show that there is no absolute advantage of one technology on the other. In fact, from the end of September to the end of February the PV power is greater than the one of PT. From the end of February till mid-April the PT power exceeds that of PV. This latter overcome again the PT power from mid-April to mid-May. From mid-May till the end of September the PT power offers much potential. Hence, the choice between the two technologies depends on the selection criterion. If the criterion is the total energy, the two systems are nearly equivalent with a negligible advantage for the PT. If the criterion is a minimum threshold power of 30kWAC, the advantage is for the PV. Finally if the criterion is to have maximum power during a predefined period, the choice is for the higher potential. The overlap between the power curves is resulting from the fact that the two systems are influenced by different parameters. For instance, parabolic troughs convert only the direct beam of radiation while photovoltaic panels are able to convert both direct and diffuse radiations into electricity. Furthermore, the temperature has opposite effect on the two technologies: the output power produced by PT is positively affected by temperature increase while PV power drops with temperature raise. For this reason, PT system is preferred during the summer due to high temperatures while PV system is better during the winter because of low temperatures. In addition, results reveal that PT power reaches its peak value in June and August while the maximum PV power occurs in June only. The reason behind this result depends on two factors. From one hand, Lebanon receives maximum radiations from June to August and from the other hand, the temperature difference between June and August is relatively big. This makes the PV power decrease from its peak value in July and August because of high temperatures. However, high temperatures are favourable for PT power during these months so PT system maintains its maximum power point except a moderate decrease in July. This decrease is caused by high levels of humidity due to the geography of the studied location near the Mediterranean Sea. High humidity in July results in a foggy weather and therefore reduces the amount

of direct radiations which cause a power drop in PT. In contrast, PV power is not hugely affected by direct radiation decrease in July because PV still benefits from diffuse radiations.

Figure 11 presents the yearly hydrogen production rates for PV and PT with 1000m^2 land area and an array composed of 1 row. It shows production rates similar to powers variation. Indeed, the AC powers are converted to DC ones using a rectifier. Therefore, the resulting DC powers are proportional to the AC ones with reduced values caused by the rectifier's losses. The hydrogen produced is also proportional to the DC power feeding the electrolyzer.

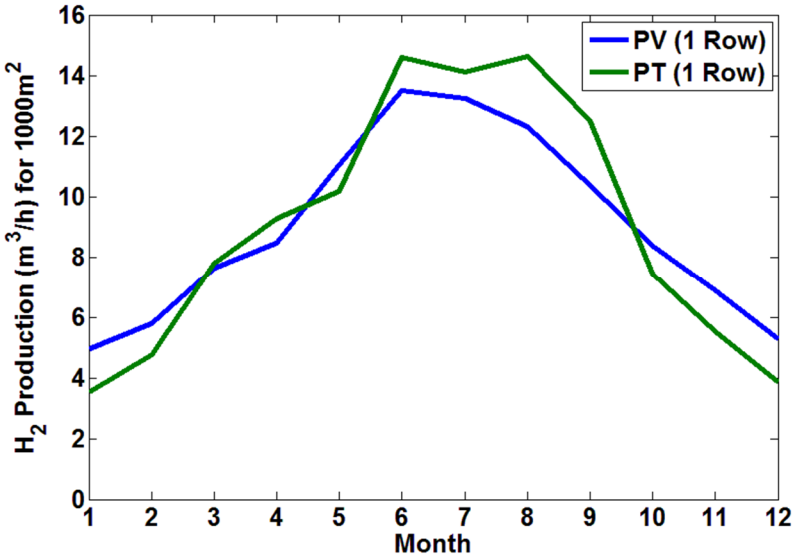

Figure 11. Yearly PV and PT H_2 production rates for 1000m^2 with 1 row.

Figure 12 show the resulting fuel cell's output powers for PV and PT. It indicates power profiles proportional to hydrogen flow rate and consequently the same analysis of AC powers behavior applies for fuel cell powers.

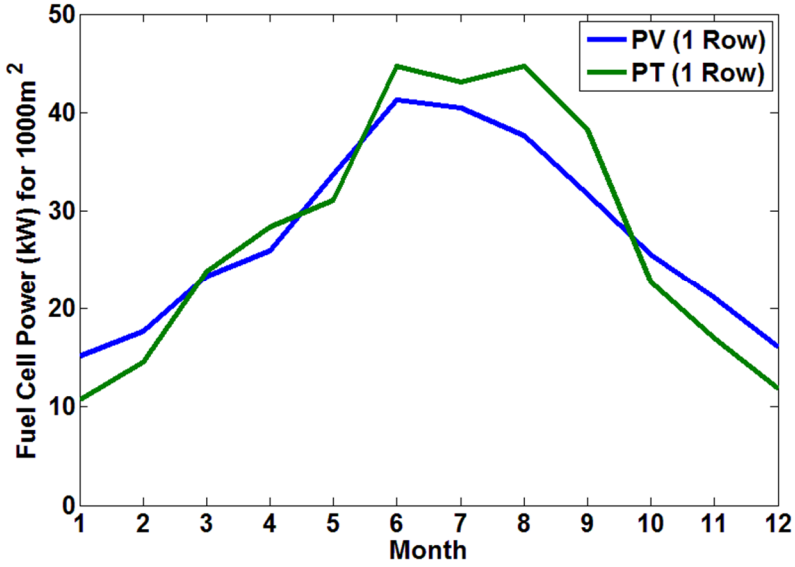

Figure 12. Yearly FC-PV and FC-PT output powers for 1000m^2 with 1 row

The effects of the land's area and the array's configuration on Fuel Cell's power for PV and PT are studied in Figures 13 to 17. In Figure 13 the effect of array's rows on FC-PV and FC-PT output

powers for 1000m^2 is shown. Here two configurations are considered: array composed of 2 rows of PV modules or parabolic troughs, as well as array of 3 rows.

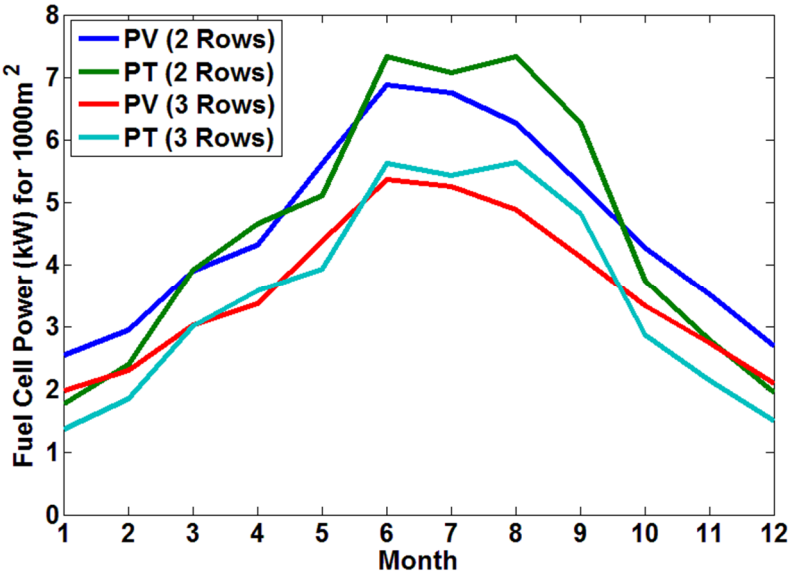

Figure 13. Effect of array's rows on FC-PV and FC-PT output powers for 1000m^2

Comparing to the results of Figure 12 (case of 1 row) we notice a significant decrease in the output powers for 2 and 3 rows. For 1 row the peak powers are 44.73kW for FC-PT and 41.25kW for FC-PV. For 2 rows the peak powers are 7.33kW for FC-PT and 6.87kW for FC-PV. In case of 3 rows the peak powers are 5.63kW for FC-PT and 5.35kW for FC-PV. The interpretation of these results is based on the spacing distance needed in case of multiple rows to avoid shading. Indeed, increasing the number of rows requires a bigger spacing distance between modules or troughs and results consequently in a loss of the effective land area. In this context, a factor called land factor LF is calculated for each case of the array's configuration. The LF is the ratio of the area occupied by the modules or troughs over the land area. The calculated land factors for different rows are: LF=1 for 1 row, LF=6 for 2 rows and LF=7.7 for 3 rows. The increase in the land factor implies less panels/troughs could be installed in the available land area and therefore less power is generated. In addition, the study of different cases reveals that the land factor increase is not proportional to the number of array's rows.

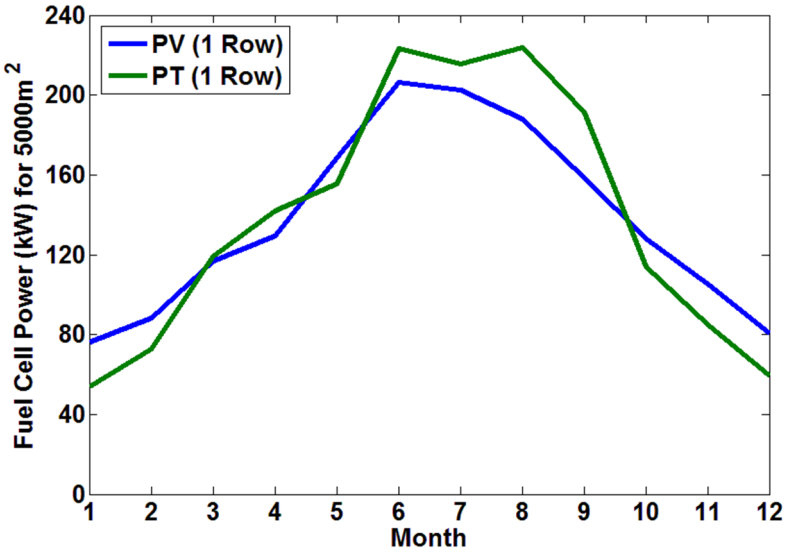

Figure 14. Yearly FC-PV and FC-PT output powers for 5000m^2 with 1 row

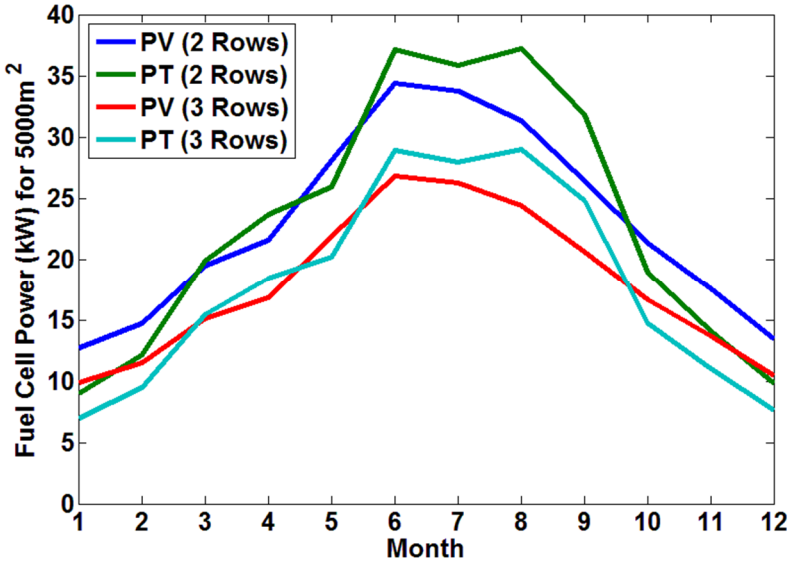

Figure 15. Effect of array's rows on FC-PV and FC-PT output powers for 5000m^2

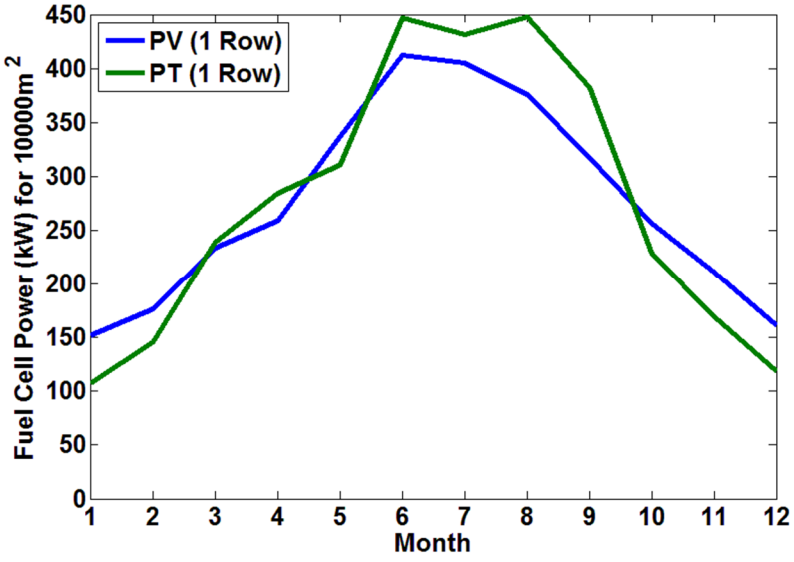

Figure 16. Yearly FC-PV and FC-PT output powers for 10000m^2 with 1 row

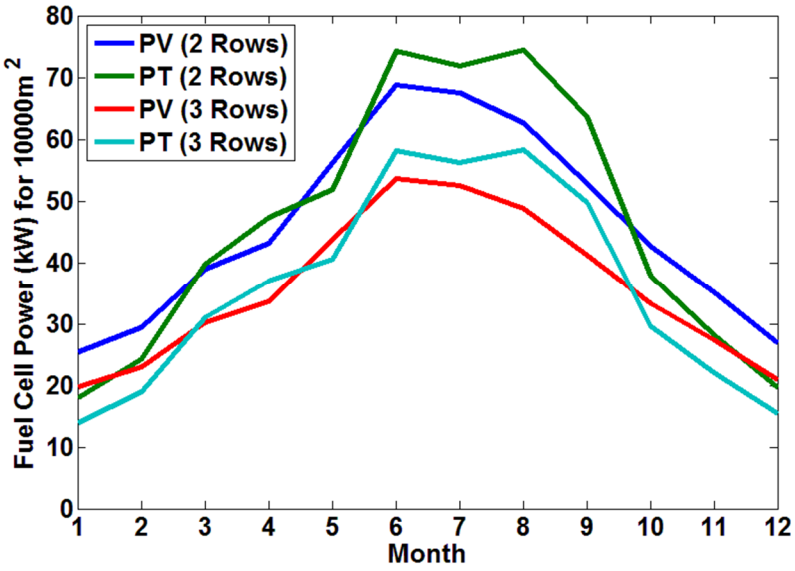

Figure 17. Effect of array's rows on FC-PV and FC-PT output powers for 10000m^2

The same analyses apply for the results of Figures 14 to 17 but with higher levels of powers due to the increase in area. Results of 5000m^2 are presented in Figures 14 (1 row) and 15 (2 and 3 rows), while results of 10000m^2 are presented in Figures 16 (1 row) and 17 (2 rows and 3 rows).

The evolution of the fuel cell's maximum power with respect to the area for different rows is shown in Figures 18 and 19. The results indicate a proportional increase of the maximum power with respect to the land area. Moreover, the results show an advantage for the FC-PT system over the FC-PV one: the slopes of PT lines are greater than the ones of PV lines for all cases of array's configuration (1 row, 2 rows and 3rows).

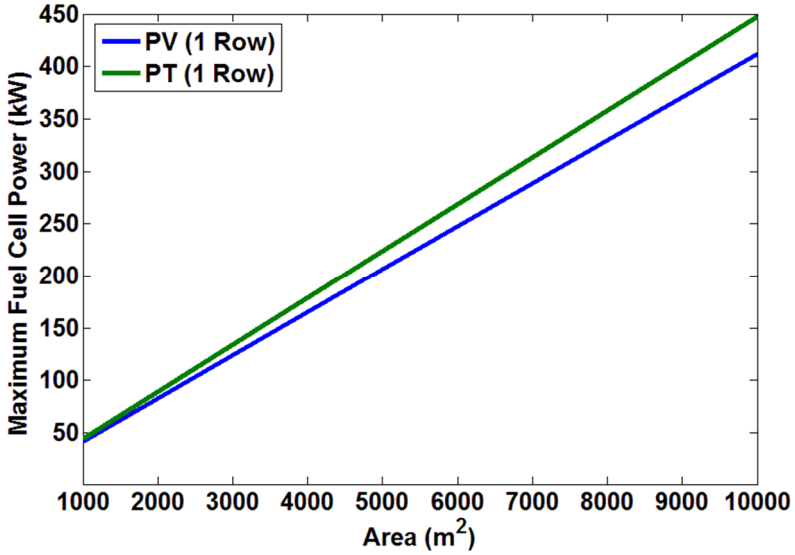

Figure 18. Maximum FC power versus land area for 1 row

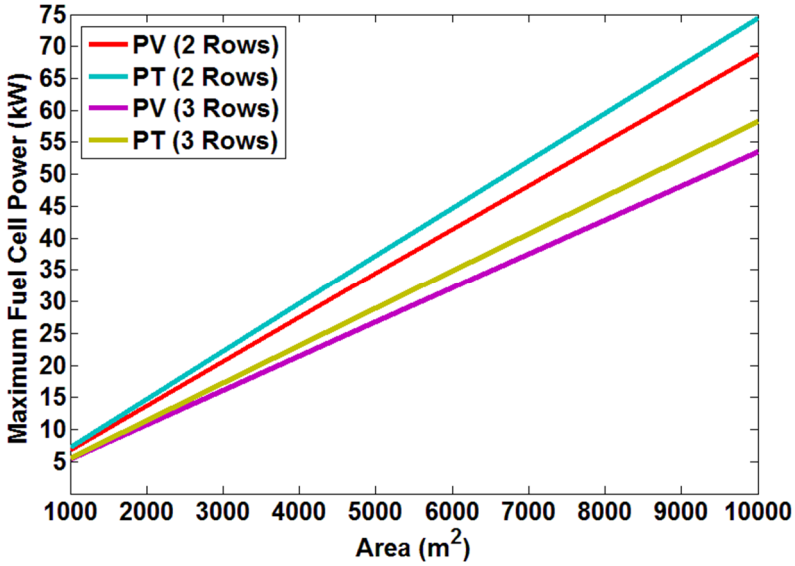

Figure 19. Maximum FC power versus land area for 2 and 3 rows

The evolution of the fuel cell's maximum power with respect to the number of rows for different areas, is shown in Figure 20. The results show a significant decrease of the maximum power from 1 row configuration to 2 rows configuration. This is due to the fact that for 1 row, the entire land area is covered with modules/troughs because of absence of shading (LF=1). However, for 2 rows the spacing distance needed to avoid shading, hugely reduces the number of modules/troughs (LF=6). Finally, the maximum power drop is limited from 2 rows configuration to 3 rows configuration. This is due to the limitation of land factor increase: here the LF is increased from 6 to 7.7 comparing to an increase from 1 to 6 in the first interval.

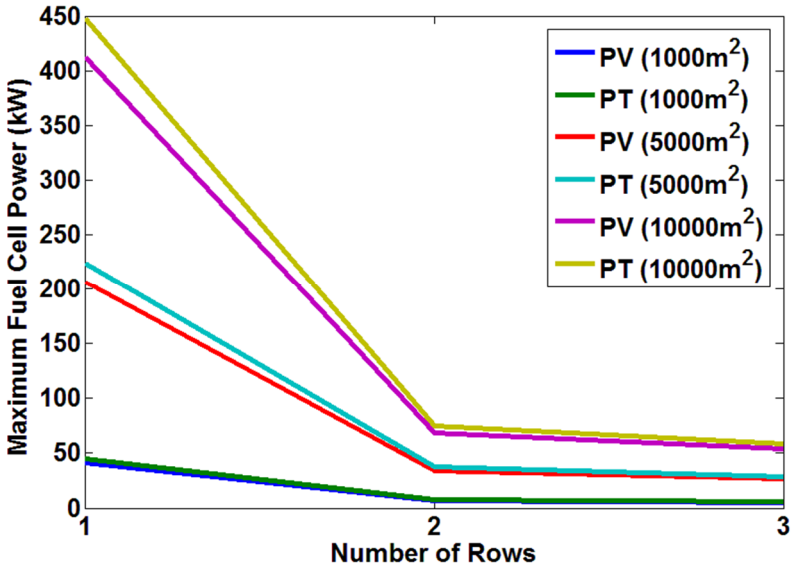

Figure 20. Maximum FC power versus number of rows for 1000m², 5000m² and 10000m²

8 CONCLUSION

The present work proposes a green-green energy system based on the coupling of Fuel Cell with PV or solar thermal system through hydrogen storage. For the case study, a 1000 m² land in the city of Tripoli (Lebanon) is considered. Mathematical models for PV array, PT system, Fuel Cell and

Electrolyzer are elaborated. Proposed models calculate the output power of each system as well as the produced quantity of hydrogen. A comparison between the output powers of the two solar systems based on yearly insulation data is performed. An optimization procedure is suggested relying on different selection criteria which can be the yearly total energy, the minimum guaranteed threshold of power or the maximum power during a fixed period. Results reveal that both systems are nearly equivalent regarding the yearly produced energy. Furthermore, results indicate that PV ensures a better minimum threshold power of 5kW. However, if the criterion is to have maximum power during the summer period, the advantage is for the solar thermal system. This is due to the fact that solar thermal system is positively affected by temperature increase in summer while PV is negatively influenced by this increase. Finally, when coupled with Fuel Cell the PV generates more power because there is no need for a rectifier to produce hydrogen as in case of solar thermal system.

REFERENCES

[1] Farouk Hachem, Bakri Abdulhay, Mohamad Ramadan, Hicham El Hage, Mostafa Gad El Rab, Mahmoud Khaled, Improving the performance of photovoltaic cells using pure and combined phase change materials – Experiments and transient energy balance, Renewable Energy, Volume 107, July 2017, Pages 567-575.

[2] Ahmad El Mays, Rami Ammar, Mohamad Hawa, Mohamad Abou Akroush, Farouk Hachem, Mahmoud Khaled, Mohamad Ramadan, Improving Photovoltaic Panel Using Finned Plate of Aluminum, Energy Procedia, Volume 119, 2017, Pages 812-817

[3] Amal Herez, Mohamad Ramadan, Mahmoud Khaled, Review on solar cooker systems: Economic and environmental study for different Lebanese scenarios, Renewable and Sustainable Energy Reviews, Volume 81, Part 1, 2018, Pages 421-432.

[4] Ahmad El Mays, Rami Ammar, Mahamad Hawa, Mahamad Abou Akroush, Farouk Hachem, Mahmoud Khaled, Mohamad Ramadan, Using phase change material in under floor heating, Energy Procedia, Volume 119, 2017, Pages 806-811.

[5] Herez A, Ramadan M, Abdulhay B, Khaled M. Short review on solar energy systems. AIP Conference Proceedings 2016; 1758: 1- 10.1063/1.4959437.

[6] Mohamad Ramadan, Rabih Murr, Mahmoud Khaled, Abdul Ghani Olabi, Mixed numerical - Experimental approach to enhance the heat pump performance by drain water heat recovery, Energy, Volume 149, 2018, Pages 1010-1021, ISSN 0360-5442, https://doi.org/10.1016/j.energy.2018.01.086.

[7] Mohamad Ramadan, Mahmoud Khaled, Ahmad Haddad, Bakri Abdulhay, Andy Durrant and Hicham El Hage, An inhouse code for simulating heat recovery from boilers to heat water Energy, https://doi.org/10.1016/j.energy.2018.05.154.

[8] Hassan Jaber, Mohamad Ramadan, Thierry lemenand, Mahmoud Khaled, Domestic thermoelectric cogeneration system optimization analysis, energy consumption and CO2 emissions reduction, Applied Thermal Engineering, Volume 130, 2018, Pages 279-295.

[9] H. Jaber, M. Khaled, T. Lemenand, M. Ramadan, Short review on heat recovery from exhaust gas AIP Conf Proc, 1758 (2016), 10.1063/1.4959441.

[10] Mahmoud Khaled, Mohamad Ramadan, Heating fresh air by hot exhaust air of HVAC systems, Case Studies in Thermal Engineering, Volume 8, 2016, Pages 398-402, ISSN 2214-157X, https://doi.org/10.1016/j.csite.2016.10.004.

[11] Mohamad Ramadan, Mahmoud Khaled, Hicham El Hage, Using Speed Bump for Power Generation –Experimental Study, Energy Procedia, Volume 75, 2015, Pages 867-872, ISSN 1876-6102, https://doi.org/10.1016/j.egypro.2015.07.192.

[12] Mahmoud Khaled, Mohamad Ramadan, Hicham El-Hage, Ahmed Elmarakbi, Fabien Harambat, Hassan Peerhossaini, Review of underhood aerothermal management: Towards vehicle simplified models, Applied Thermal Engineering, Volume 73, Issue 1, 2014, Pages 842-858, ISSN 1359-4311, https://doi.org/10.1016/j.applthermaleng.2014.08.037.

[13] T Wilberforce, A Alaswad, A Palumbo, M Dassisti, AG Olabi, Advances in stationary and portable fuel cell applications, 2016 International Journal of Hydrogen Energy 41 (37), 16509-16522.

[14] A Alaswad, A Baroutaji, H Achour, J Carton, A Al Makky, AG Olabi, Developments in fuel cell technologies in the transport sector, 2015 International Journal of Hydrogen Energy 41 (37), 16499-16508.

[15] JG Carton, AG Olabi, Representative model and flow characteristics of open pore cellular foam and potential use in proton exchange membrane fuel cells, 2015 International Journal of Hydrogen Energy 40 (16), 5726-5738.

[16] AM Oladoye, JG Carton, K Benyounis, J Stokes, AG Olabi, Optimisation of pack chromised stainless steel for proton exchange membrane fuel cells bipolar plates using response surface methodology, 2016, Surface and Coatings Technology 304, 384-392.

[17] Yusuf Bicer, Ibrahim Dincer, Clean fuel options with hydrogen for sea transportation: A life cycle approach, International Journal of Hydrogen Energy, Volume 43, Issue 2, 11 January 2018, Pages 1179-1193, ISSN 0360-3199, https://doi.org/10.1016/j.ijhydene.2017.10.157.

[18] Anwar Hammad, Ibrahim Dincer, Analysis and assessment of an advanced hydrogen liquefaction system, International Journal of Hydrogen Energy, Volume 43, Issue 2, 11 January 2018, Pages 1139-1151, ISSN 0360-3199.

[19] Yunus Emre Yuksel, Murat Ozturk, Ibrahim Dincer, Energetic and exergetic performance evaluations of a geothermal power plant based integrated system for hydrogen production,

International Journal of Hydrogen Energy, Volume 43, Issue 1, 4 January 2018, Pages 78-90, ISSN 0360-3199, https://doi.org/10.1016/j.ijhydene.2017.11.002.

[20] Yildiz Kalinci, Ibrahim Dincer, Analysis and performance assessment of NH3 and H2 fed SOFC with proton-conducting electrolyte, International Journal of Hydrogen Energy, Volume 43, Issue 11, 15 March 2018, Pages 5795-5807, ISSN 0360-3199, https://doi.org/10.1016/j.ijhydene.2017.07.234.

[21] Canan Acar, Ibrahim Dincer, Thermodynamic analysis and experimental investigation of a unique photoelectrochemical hydrogen production system, International Journal of Hydrogen Energy, Volume 43, Issue 9, 1 March 2018, Pages 4223-4232, ISSN 0360-3199, https://doi.org/10.1016/j.ijhydene.2017.07.043.

[22] Minghong Huang, Liuzhang Ouyang, Hui Wang, Jiangwen Liu, Min Zhu, Hydrogen generation by hydrolysis of MgH2 and enhanced kinetics performance of ammonium chloride introducing, International Journal of Hydrogen Energy, Volume 40, Issue 18, 2015, Pages 6145-6150, ISSN 0360-3199, https://doi.org/10.1016/j.ijhydene.2015.03.058.

[23] L.Z. Ouyang, Z.J. Cao, L.L. Li, H. Wang, J.W. Liu, D. Min, Y.W. Chen, F.M. Xiao, R.H. Tang, M. Zhu, Enhanced high-rate discharge properties of La11.3Mg6.0Sm7.4Ni61.0Co7.2Al7.1 with added graphene synthesized by plasma milling, International Journal of Hydrogen Energy, Volume 39, Issue 24, 2014, Pages 12765-12772, ISSN 0360-3199, https://doi.org/10.1016/j.ijhydene.2014.06.111.

[24] L. Z. Ouyang, X. S. Yang, M. Zhu, J. W. Liu, H. W. Dong, D. L. Sun, J. Zou, and X. D. Yao. Enhanced Hydrogen Storage Kinetics and Stability by Synergistic Effects of in Situ Formed CeH2.73 and Ni in CeH2.73-MgH2-Ni Nanocomposites The Journal of Physical Chemistry C 2014 118 (15), 7808-7820DOI: 10.1021/jp500439n.

[25] H. Zhong, H. Wang, J.W. Liu, D.L. Sun, F. Fang, Q.A. Zhang, L.Z. Ouyang, M. Zhu, Enhanced hydrolysis properties and energy efficiency of MgH2-base hydrides, Journal of Alloys and Compounds, Volume 680,2016, Pages 419-426, ISSN 0925-8388, https://doi.org/10.1016/j.jallcom.2016.04.148.

[26] L.Z. Ouyang, H. Zhong, Z.M. Li, Z.J. Cao, H. Wang, J.W. Liu, X.K. Zhu, M. Zhu, Low-cost method for sodium borohydride regeneration and the energy efficiency of its hydrolysis and regeneration process, Journal of Power Sources, Volume 269, 2014, Pages 768-772, ISSN 0378-7753, https://doi.org/10.1016/j.jpowsour.2014.07.074.

[27] Zhijie Cao, Liuzhang Ouyang, Hui Wang, Jiangwen Liu, Dalin Sun, Qingan Zhang, Min Zhu, Advanced high-pressure metal hydride fabricated via Ti–Cr–Mn alloys for hybrid tank, International Journal of Hydrogen Energy, Volume 40, Issue 6, 2015, Pages 2717-2728, ISSN 0360-3199, https://doi.org/10.1016/j.ijhydene.2014.12.093.

[28] Zhijie Cao, Liuzhang Ouyang, Lingling Li, Yanshan Lu, Hui Wang, Jiangwen Liu, De Min, Yanwen Chen, Fangming Xiao, Tai Sun, Renheng Tang, Min Zhu, Enhanced discharge capacity and cycling properties in high-samarium, praseodymium/neodymium-free, and low-cobalt A2B7 electrode materials for nickel-metal hydride battery, International Journal of Hydrogen Energy, Volume 40, Issue 1, 2015, Pages 451-455, ISSN 0360-3199, https://doi.org/10.1016/j.ijhydene.2014.11.016.

[29] Yunfei Yan, Zhien Zhang, Li Zhang, Xin Wang, Ke Liu, Zhongqing Yang, Investigation of autothermal reforming of methane for hydrogen production in a spiral multi-cylinder micro-reactor used for mobile fuel cell, International Journal of Hydrogen Energy, Volume 40, Issue 4, 2015, Pages 1886-1893, ISSN 0360-3199, https://doi.org/10.1016/j.ijhydene.2014.11.140.

[30] Samia Bensmail, Djamila Rekioua, Halim Azzi, Study of hybrid photovoltaic/fuel cell system for stand-alone applications, International Journal of Hydrogen Energy, Volume 40, Issue 39, 19 October 2015, Pages 13820-13826, ISSN 0360-3199.

[31] Ekin Özgirgin, Yılser Devrim, Ayhan Albostan, Modeling and simulation of a hybrid photovoltaic (PV) module-electrolyzer-PEM fuel cell system for micro-cogeneration applications, International Journal of Hydrogen Energy, Volume 40, Issue 44, 26 November 2015, Pages 15336-15342, ISSN 0360-3199, https://doi.org/10.1016/j.ijhydene.2015.06.122.

[32] I. Tegani, A. Aboubou, M.Y. Ayad, R. Saadi, M. Becherif, M. Bahri, M. Benaouadj, O. Kraa, Experimental validation of differential flatness-based control applied to stand alone using photovoltaic/fuel cell/battery hybrid power sources, International Journal of Hydrogen Energy, Volume 42, Issue 2, 12 January 2017, Pages 1510-1517, ISSN 0360-3199, https://doi.org/10.1016/j.ijhydene.2016.06.081.

[33] M.F. Ezzat, I. Dincer, Development, analysis and assessment of fuel cell and photovoltaic powered vehicles, International Journal of Hydrogen Energy, Volume 43, Issue 2, 11 January 2018, Pages 968-978, ISSN 0360-3199, https://doi.org/10.1016/j.ijhydene.2017.05.065.

[34] Pouria Ahmadi, Ibrahim Dincer, Marc A. Rosen, Transient thermal performance assessment of a hybrid solar-fuel cell system in Toronto, Canada, International Journal of Hydrogen Energy, Volume 40, Issue 24, 29 June 2015, Pages 7846-7854, ISSN 0360-3199, https://doi.org/10.1016/j.ijhydene.2014.11.047.

[35] M. Ramadan, M. Khaled, H.S. Ramadan, M. Becherif, Modeling and sizing of combined fuel cell-thermal solar system for energy generation, International Journal of Hydrogen Energy, Volume 41, Issue 44, 26 November 2016, Pages 19929-19935, ISSN 0360-3199, https://doi.org/10.1016/j.ijhydene.2016.08.222.

[36] Ahmad Haddad, Mohamad Ramadan, Mahmoud Khaled and Khaled Chahine, An investigation on coupling fuel cell and photovoltaic systems for power generation, 3rd International

Conference on Advances in Computational Tools for Engineering Applications (ACTEA), 13-15 July 2016 – Beirut, Lebanon.

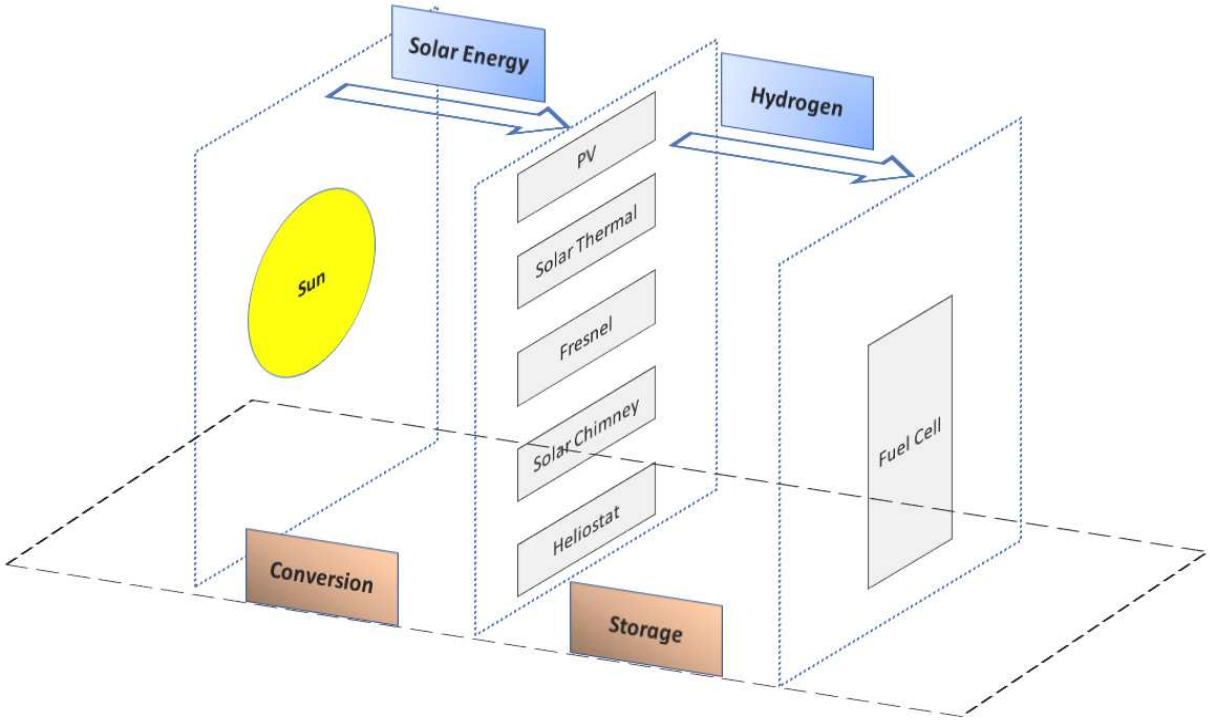
Solar Energy
Hydrogen
PV
Solar Thermal
Fresnel
Solar Chimney
Heliostat
sun
Fuel Cell
Conversion
Storage